RESEARCH ARTICLE

WILEY

A comparison of Lenz lenses and LC resonators for NMR signal enhancement

Mazin Jouda[1] | **Robert Kamberger[2]** | **Jochen Leupold[3]** | **Nils Spengler[4]** | **Jürgen Hennig[3]** | **Oliver Gruschke[5]** | **Jan G. Korvink[1]**

[1]Karlsruhe Institute of Technology-KIT, Institute of Microstructure Technology-IMT, Eggenstein-Leopoldshafen, Germany

[2]BrainLinks-BrainTools Cluster of Excellence, Institute of Microsystems Technology-IMTEK, University of Freiburg, Freiburg, Germany

[3]Department of Radiology, Medical Physics, Medical Center - University of Freiburg, Faculty of Medicine, University of Freiburg, Freiburg, Germany

[4]RF360 Europe GmbH, Munich, Germany

[5]Bruker BioSpin GmbH, Rheinstetten, Germany

Correspondence
J. G. Korvink, Karlsruhe Institute of Technology-KIT, Institute of Microstructure Technology-IMT, Eggenstein-Leopoldshafen, Germany.
Email: jan.korvink@kit.edu

Funding information
European Research Council, Grant/Award Number: 290586; German Research Foundation, Grant/Award Number: EXC 1086

Abstract

High signal-to-noise ratio (SNR) of the NMR signal has always been a key target that drives massive research effort in many fields. Among several parameters, a high filling factor of the MR coil has proven to boost the SNR. In case of small-volume samples, a high filling factor and thus a high SNR can be achieved through miniaturizing the MR coil. However, under certain circumstances, this can be impractical. In this paper, we present an extensive theoretical and experimental investigation of the inductively coupled LC resonator and the magnetic Lenz lens as two candidate approaches that can enhance the SNR in such circumstances. The results demonstrate that the narrow-band LC resonator is superior in terms of SNR, while the non-tuned nature of the Lenz lens makes it preferable in broadband applications.

KEYWORDS
inductive coupling, LC resonator, Lenz lens, NMR

1 | INTRODUCTION

Inductive coupling is often used in magnetic resonance imaging (MRI) and spectroscopy (MRS). Two inductances are inductively coupled if they are arranged in such a way that flux lines of one inductance penetrates the area enclosed by the other inductance and thus share a mutual inductance (M) as shown in Figure 1.

Jouda, Kamberger, and Gruschke contributed equally to the paper.

In magnetic resonance, the inductive coupling effect has been used for two applications: (i) Tuning and matching of MR detectors, which is achieved by placing an external inductance close to the MR detector. By changing the inductance's relative position the mutual inductance is modified and which modifies the detector's resonance frequency.[1-6] (ii) The wireless transfer of energy (signal) from an MR detector, which is enabled by placing a pick-up coil which is wired to the spectrometer in close proximity to a non-wired MR detector. The signal recorded by the MR detector
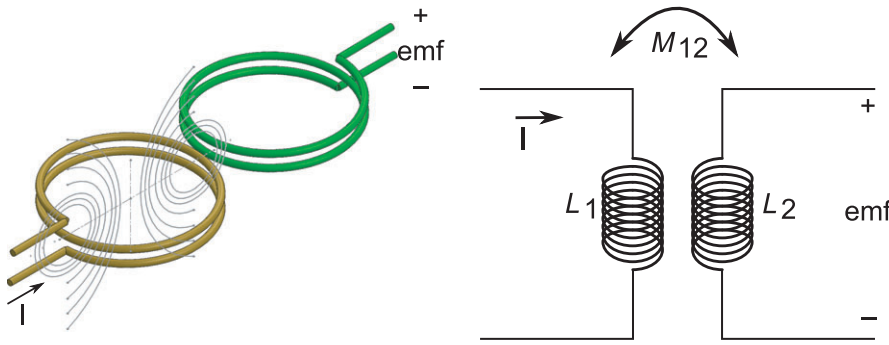
FIGURE 1 Flux linkage between two coils and their equivalent circuit

is transferred via inductive coupling to the spectrometer and is typically used to access samples within restricted areas,[7-13] to locally enhance the signal-to-noise ratio (SNR),[14-16] or to improve the handling comfort of MR probes.[17-22]

The magnetic coupling between inductors is described by Faraday's law of induction:

$$\text{emf} = -\frac{d\Phi_B}{dt} \tag{1}$$

where the electromotive force, emf, is the magnetic flux Φ_B per time t. The magnetic flux depends on the enclosed area A and the magnetic flux density B($d\Phi_B = d(A \cdot B)$). The signal transfer between the inductances depends on the magnitude of the magnetic flux density which is, in turn, proportional to the electric current ($B(i)$) in the primary circuit, and on the percentage of field lines linked to the secondary, which is proportional to the area (A) enclosed by the secondary inductance.

To ensure maximum signal transfer, the emf in the secondary coil is boosted by placing a capacitor in parallel with the inductance L_2. Thus, the circuit resonates at the Larmor frequency. This resonant inductive coupling configuration poses certain constraints on the MR detector design and its application.

The resonance frequency of the secondary circuit depends, besides its own parameters such as coil geometry and capacitor, on the load, that is, the sample, and the primary circuit through the mutual inductance. Thus, the LC resonator typically functions only with a dedicated primary coil and sample, and cannot be used efficiently when the loading conditions are altered. Due to possible occurrence of splitting,[23] a large range for tuning and matching is of necessity. Thus, an implementation within an existing system (primary) is problematic, especially considering the reduced tuning and matching range, which reduces the adjustability for different loads and thus limits the range of examinable samples. Besides these disadvantages, a simple LC resonator only transmits a single frequency with high efficiency, and thus can only be used with limitations within a multiresonant primary coil.[24-26]

An alternative approach to locally enhance SNR is to use the so-called Lenz lenses. A Lenz lens, as introduced by Schoenmaker et al,[27] consists of a single current carrying track, with an outer and an inner loop. Since in a Lenz lens, there is a single current carrying track, the outer loop of the Lenz lens carries the opposing current, while the current direction of the inner loop has the same direction as the source current. Since the magnetic flux density (B-field) in a current loop depends on the current and the radius of the loop, the magnetic flux density is higher in the inner loop, and thus, the magnetic flux is focused in a smaller area of interest.

In this paper, we will introduce a thorough comparison, supported by Matlab simulations, derived formulas, and experiments, of the various approaches utilized to enhance the sensitivity of the MR probe. First, we will describe the small wired probe (SWP) with inductance $L_{a,S}$ and resistance $r_{a,S}$. This coil has the same geometry as the sample, thus achieves highest filling factor and therefore it will be used as a reference. Then, we will introduce the big wired probe (BWP), with inductance $L_{a,B}$ and resistance $r_{a,B}$, that shows how the sensitivity decays as the filling factor gets lower. After that, we show how the LC resonator, with inductance L_c, resistance r_c, and capacitance C_c, can enhance the sensitivity of the BWP. Finally, we introduce the lenz lens (LL), with outer loop inductance L_b and inner loop inductance L_c, as an alternative method to enhance the sensitivity of the BWP. These four coil configurations are summarized in Table 1.

2 | THEORY

2.1 | Simulation

In this section, we analyze the circuit models for the various coil configurations and explore the differences in performance via simulating these circuits in Matlab.

2.1.1 | Wired probe

First, we will consider the case when the MR probe is directly connected to the MR receiver. Figure 2 depicts a typical circuit model of the NMR probe. It shows the

TABLE 1 Summary of the various coil configurations

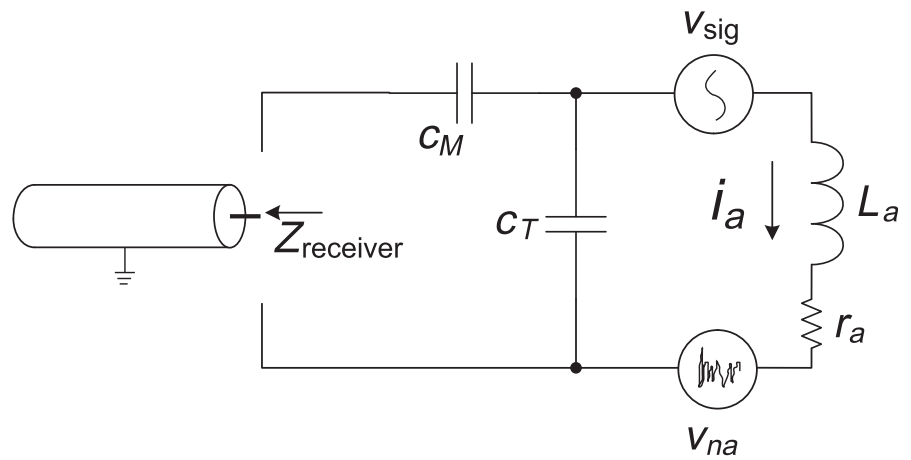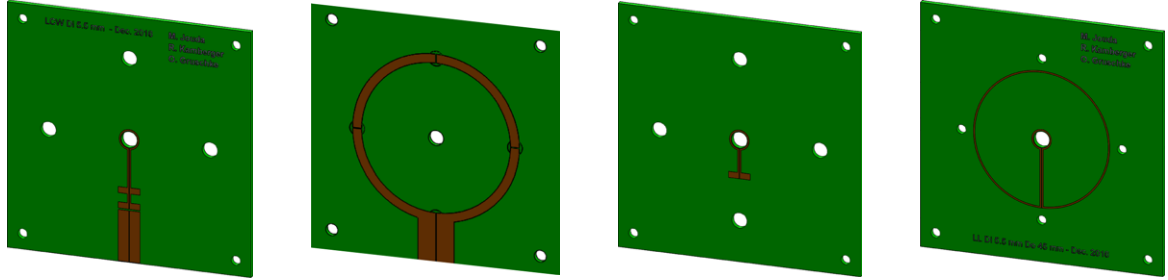|	SWP	BWP	LC resonator	Lenz lens
Inductance	$L_{a,S}$	$L_{a,B}$	L_c	L_b, L_c
Resistance	$r_{a,S}$	$r_{a,B}$	r_c	r_b, r_c
Capacitance	-	-	C_c	-
Diameter	$D_{a,S}$	$D_{a,B}$	D_c	D_b, D_c

FIGURE 2 Typical NMR probe circuit with the associated tuning and matching capacitors. The circuit additionally shows the source models of the NMR signal as well as the noise

detection coil shunted with a tuning capacitor C_T, which tunes the coil in a way such that it resonates slightly above the Larmor frequency and the real part of the parallel LC is 50 Ohms. This is formulated mathematically as

$$\{1/(j\omega * C_T)\|r_a + j\omega * L_a\} = 50 + jX. \tag{2}$$

The value of C_T can then be readily obtained from the above equation by solving only the real part of the equation. The residual imaginary part of the equation is inductive in this case and can therefore be eliminated by the matching capacitor C_M through solving the imaginary part of the following equation

$$\{1/(j\omega * C_T)\|r_a + j\omega * L_a\} + 1/(j\omega * C_M) = 50. \tag{3}$$

The voltage source v_{sig}, in Figure 2, represents the voltage of the NMR signal induced in the detection coil L_a. This can be calculated from the reciprocity principle[28] for a 90° flip angle as follows

$$v_{sig} = K\omega_0 B_u V_s M_0 \tag{4}$$

where K is a factor that takes into account the inhomogeneity of B_u, ω_0 is the Larmor frequency, B_u is the transverse

magnetic field of the coil when a 1 A current flows through it, V_s is the sample volume, and M_0 is the net magnetization which can be derived from the following expression

$$M_0 = \frac{N\gamma^2\hbar^2 I(I+1)B_0}{3kT_s} \tag{5}$$

in which N is the number of spins within the sample, γ is the magnetogyric ratio, $\hbar$ is the reduced Planck constant, I is the spin quantum number, k is the Boltzmann constant, and T_s is the sample temperature. The thermal noise associated with the NMR signal is modeled in Figure 2 by a voltage source v_n, whose amplitude is determined from the following formula

$$v_n = \sqrt{4kT_c\Delta fR} \tag{6}$$

with T_c being the coil temperature, Δf the receiver bandwidth, and R the AC resistance of the coil including the skin and proximity effects.

Obviously, according to the above equations, the SNR depends upon several parameters. However, for a fixed
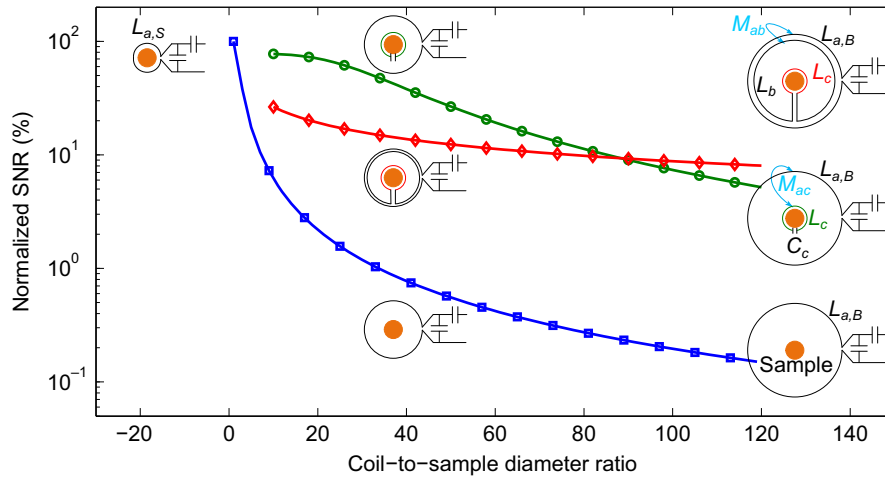
FIGURE 3 Effect of increasing the coil-to-sample diameter ratio. (The blue curve with square markers): effect of increasing the diameter of the detection coil for a fixed sample volume on the SNR. (The green curve with circle markers): effect of increasing the detection coil's diameter on the performance of the LC resonator used to enhance the NMR SNR. In this case, the inner coil, L_c, has a fixed diameter equal to that of the sample. (The red curve with rhombus markers): effect of increasing the detection coil's diameter on the performance of the LL used to enhance the NMR SNR. In this case, the inner coil of the LL, L_c, has a fixed diameter equal to that of the sample, while the outer coil, L_b, has a diameter equal to that of the detection coil

sample volume and receiver bandwidth, it is the coil geometry that plays the major role in SNR. Needless to say, regardless of the coil type, the coil windings should be as close as possible to sample so that it encounters higher B_u, and as a result, a boosted SNR can be gained. This effect is demonstrated in Figure 3 by the blue curve with square markers. For this curve, the x-axis represents the ratio between the coil and sample diameters as the coil diameter increases while the wire width and thickness are kept constant. The y-axis shows the SNR relative to that when the coil and sample diameters are equal. The SNR, in this case, is obtained via simulating the circuit in Figure 2 excluding the noise of the RF receiver, and assuming a spherical sample of water with diameter $d_{sample}=D_{a,S}$, and single-loop surface coil with diameter D_a. The steep SNR degradation in this case is mainly due to the increased AC resistance of the coil thus increased noise on the

one hand, and on the other hand due to the decrease in B_u at the sample's position.

2.1.2 | NMR probe with LC resonator

As depicted by the blue curve with square markers in Figure 3, the SNR degrades largely when the diameter of the detection coil increases. This leads to the conclusion that we should always aim at a maximum filling factor. However, in certain cases, as for example, for bench-top NMR spectrometers, the detector is non-changeable, and therefore, it is not feasible to replace such detector with one that exhibits a higher filling factor for small samples. A very good solution to such a problem is the use of a passive LC resonator.[19] The inductor L_c, in this case, is designed to achieve maximum filling factor of the sample, while the
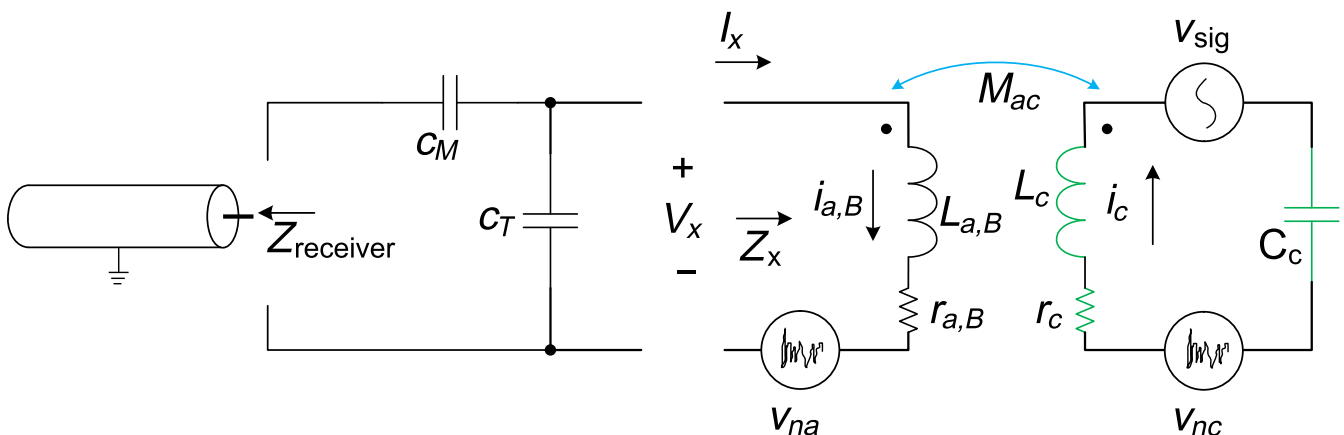

FIGURE 4 Circuit model of an NMR probe with LC resonator for SNR enhancement
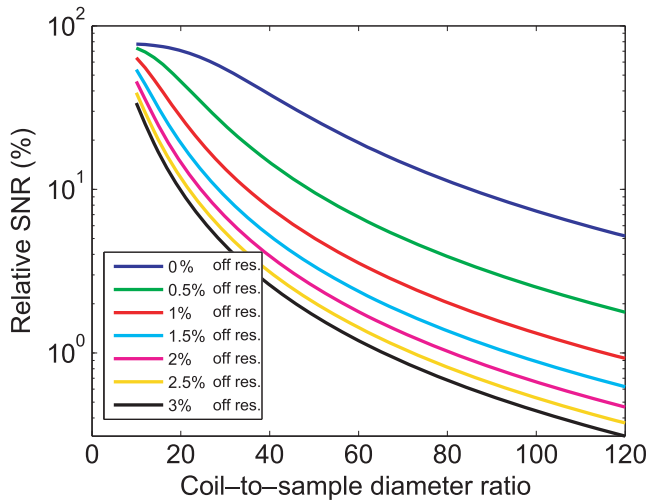
FIGURE 5 Effect of resonance frequency deviation on the performance of the LC resonator [Colour figure can be viewed at wileyonlinelibrary.com]

capacitor C_c is chosen in a way to make the L_c resonate at the Larmor frequency $C_c = 1/(L_c\omega^2)$. Figure 4 shows the schematic diagram of the circuit model for an NMR probe with an LC resonator. Once the LC resonator is inserted inside the NMR probe, the tuning and matching will be disturbed due to the mutual inductance. The updated values of C_T and C_M can be recalculated via the following three equations

$$Z_x = \frac{V_x}{I_x} = r_{a,B} + j\omega L_{a,B} - \frac{(j\omega M_{ac})^2}{r_c + j\omega L_c + \frac{1}{j\omega C_c}}, \qquad (7)$$

$$\Re\left[\frac{Z_x \cdot \frac{1}{j\omega C_T}}{Z_x + \frac{1}{j\omega C_T}}\right] = 50, \qquad (8)$$

$$\Im\left[\frac{1}{j\omega C_M} + \frac{Z_x \cdot \frac{1}{j\omega C_T}}{Z_x + \frac{1}{j\omega C_T}}\right] = 0. \qquad (9)$$

After updating the values of the tuning and matching capacitors, the SNR can be calculated (excluding the noise of

the RF receiver) directly by simulating the circuit and applying the superposition principle to find the overall noise due to individual contribution from each resistance. Worthy to remember, it is the noise powers which add, and not the voltages. Thus, the overall noise voltage is $V_n = \sqrt{V_{na}'^2 + V_{nc}'^2}$, where V_{na}' and V_{nc}' represent the noise contribution of r_a and r_c respectively at the probe terminals.

The green curve with circle markers in Figure 3 shows the SNR enhancement that can be attained through the use of an LC resonator. Moreover, it demonstrates how the efficiency of such resonator degrades when the diameter of the detection coil increases while the sample diameter (which is equal to the LC coil diameter) is fixed. This performance drop is due to the coupling between the coils which gets poorer with an increase in the detection coil's diameter. Nevertheless, the LC resonator still provides significant enhancement even with large coil-to-sample diameter ratio. This is true as long as the LC resonator is tuned to the Larmor frequency, which is usually not a straightforward task if we consider the coil loading and the frequency splitting due to the mutual inductance. The effect of the resonance frequency deviation from the Larmor frequency is demonstrated in Figure 5.

2.1.3 | NMR probe with Lenz lens

The LC resonator, as demonstrated in the previous subsection, is essentially a narrow band solution that is highly sensitive to frequency deviation. Therefore, if one wants to operate the LC resonator in different magnets then one repeatedly has to go through a tedious process of tuning. Furthermore, for extremely large detection coils, compared to sample's geometry, the efficacy of the LC resonator decreases remarkably, particularly if the resonator is not exactly at the Larmor frequency. These major drawbacks of the LC resonator make it useless in certain circumstances. Surprisingly, on the other hand, a non-tuned wideband magnetic Lenz lens (LL) can provide adequate SNR enhancement in such circumstances where the LC resonator
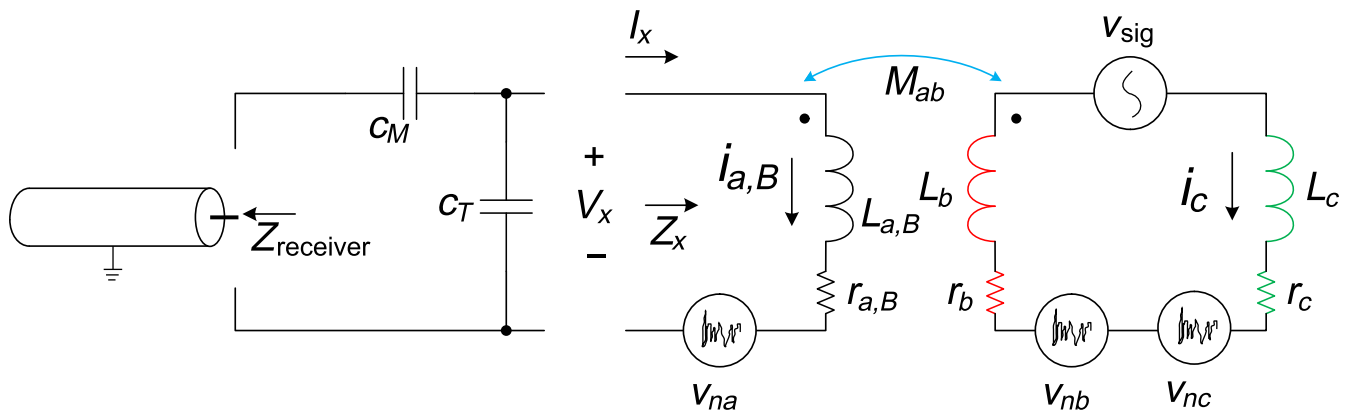

FIGURE 6 Circuit model of NMR probe with a Lenz lens for SNR enhancement

fails. The LL comprises two electrically connected coils: the inner coil, L_c, which is usually designed in a way such that it achieves high filling factor of the sample, and the outer coil, L_b, which is designed in a way to achieve maximum inductive coupling with the detection coil, $L_{a,B}$. Due to high coupling, L_b collects the majority of the flux of $L_{a,B}$, and converts it to a large current. This current flows in L_c resulting in a high B_u field focused in the sample. As a result of the reciprocity principle, the high B_u field yields a high NMR signal induced in L_c and coupled afterwards to $L_{a,B}$ through L_b. Figure 6 depicts the circuit model of an NMR probe with a LL. The detection coil as well as the outer loop of the LL are usually way larger than the inner loop, therefore, the mutual inductances M_{ac} and M_{bc} can be simply ignored while still retaining a high fidelity of calculation. Owing to being non-tuned, the LL introduces no resonance splitting and thus renders the tuning and matching of the detection coil much relaxed. The impedance of the detection coil coupled with the LL, Z_x, is found as

$$Z_x = \frac{V_x}{I_x} = r_{a,B} + j\omega L_{a,B} - \frac{(j\omega M_{ab})^2}{r_b + r_c + j\omega L_b + j\omega L_c}. \quad (10)$$

Once Z_x is computed, the tuning and matching capacitors can be updated using Equations 8 and 9, respectively. After that, the SNR is found by solving the circuit applying the superposition principle and excluding the noise of the RF receiver. The overall noise voltage at the probe terminals is then $V_n = \sqrt{V_{na}'^2 + V_{nb}'^2 + V_{nc}'^2}$, with V_{na}', V_{nb}', and V_{nc}' being the noise contribution of the intrinsic resistances r_a, r_b, and r_c referred to the probe terminals.

The red curve with rhombus markers in Figure 3 demonstrates the achievable SNR enhancement due to the LL. It shows also the effect of increasing the diameter of the detection coil together with the outer coil of the LL on its performance. Interestingly, the figure shows that for a large (>90) coil-to-sample diameter ratio, the LL outperforms the LC resonator.

2.2 | Calculation

In this section, we will derive abstracted mathematical formulae that describe the relative SNR of the various coil configurations compared with the SWP. These generalized formulae are functions of the coils' geometry and parameters, and independent of the sample's type and volume.

2.2.1 | Wired Probe

The sensitivity of the coil in Figure 2 is described by the following equation[19,28]

$$\text{SNR}_a \propto \frac{B_a}{I_a \sqrt{r_a}}. \quad (11)$$

For the case of a single-loop planar coil with diameter D_a, Equation 11 becomes

$$\text{SNR}_a \propto \frac{1}{D_a \sqrt{r_a}}. \quad (12)$$

From this equation, the SNR of the BWP relative to that of the SWP can be calculated as

$$\frac{\text{SNR}_{\text{BWP}}}{\text{SNR}_{\text{SWP}}} = \frac{\text{SNR}_{a,B}}{\text{SNR}_{a,S}} = \frac{D_{a,S}\sqrt{r_{a,S}}}{D_{a,B}\sqrt{r_{a,B}}}. \quad (13)$$

2.2.2 | NMR probe with LC resonator

Considering the circuit in Figure 4 of the probe with an LC resonator, if the resonator is tuned to the Larmor frequency, $j\omega L_c = 1/(j\omega C_c)$, then the real part of Equation 7 reduces to

$$\Re[Z_x] = r_{a,B}(1 + K_{ac}^2 Q_{a,B} Q_c) \quad (14)$$

where K_{ab} is the coupling factor between coils, $Q_{a,B}$ is the quality factor of $L_{a,B}$, and Q_c is the quality factor of L_c. Thus, the SNR of the probe with LC resonator can be calculated for a planar single-loop detection coil L_c with diameter D_c as

$$\text{SNR}_{\text{LC}} \propto \frac{B_c}{I_{a,B}\sqrt{r_{a,B}(1 + K_{ac}^2 Q_{a,B} Q_c)}}$$
$$\propto \frac{I_c / D_c}{I_{a,B}\sqrt{r_{a,B}(1 + K_{ac}^2 Q_{a,B} Q_c)}}. \quad (15)$$

The relation between I_c and $I_{a,B}$ can be straightforwardly found from Figure 4 as follows

$$\left| \frac{I_c}{I_{a,B}} \right| = \frac{\omega M_{ac}}{r_c} \quad (16)$$

which, upon insertion into Equation 15, results in

$$\text{SNR}_{\text{LC}} \propto \frac{K_{ac}\sqrt{Q_{a,B} Q_c}}{D_c \sqrt{r_c}\sqrt{1 + K_{ac}^2 Q_{a,B} Q_c}}. \quad (17)$$

Remembering that the coils L_c and $L_{a,S}$ have the same geometry, thus $D_c = D_{a,S}$, and $r_c = r_{a,S}$. Therefore, the SNR of the BWP with LC resonator relative to that of the SWP can be found as

$$\frac{\text{SNR}_{\text{LC}}}{\text{SNR}_{\text{SWP}}} = \frac{\text{SNR}_{\text{LC}}}{\text{SNR}_{a,S}} = \frac{K_{ac}\sqrt{Q_{a,B} Q_c}}{\sqrt{1 + K_{ac}^2 Q_{a,B} Q_c}}. \quad (18)$$

2.2.3 | NMR probe with Lenz lens

In Figure 6, the impedance Z_x was given by Equation 10. Thus, the real part of Z_x will be

$$\Re[Z_x] = r_{a,B} + \frac{\omega^2 M_{ab}^2 (r_b + r_c)}{(r_b + r_c)^2 + (\omega L_b + \omega L_c)^2}. \qquad (19)$$

Thus, the sensitivity of the BWP with the LL, that has a single-loop inner coil whose diameter is D_c, is calculated as

$$\mathrm{SNR_{LL}} \propto \frac{B_c}{I_{a,B}\sqrt{r_{a,B} + \frac{\omega^2 M_{ab}^2 (r_b+r_c)}{(r_b+r_c)^2 + (\omega L_b + \omega L_c)^2}}}$$

$$\propto \frac{I_c/D_c}{I_{a,B}\sqrt{r_{a,B} + \frac{\omega^2 M_{ab}^2 (r_b+r_c)}{(r_b+r_c)^2 + (\omega L_b + \omega L_c)^2}}}. \qquad (20)$$

The relation between I_c and $I_{a,B}$ can be directly found from the circuit model of the LL as follows

$$\left|\frac{I_c}{I_{a,B}}\right| = \frac{\omega M_{ab}}{\sqrt{(r_b+r_c)^2 + \omega^2 (L_b + L_c)^2}}. \qquad (21)$$

After substituting Equation 21 and performing some mathematical manipulations, Equation 20 reduces to

$$\mathrm{SNR_{LL}} \propto \frac{K_{ab}\sqrt{Q_{a,B}Q_b}}{D_c\sqrt{r_b + r_c}\sqrt{\left(\frac{r_b+r_c}{r_b}\right)(1 + Q_{LL}^2) + K_{ab}^2 Q_{a,B}Q_b}}$$

$$(22)$$

where $Q_{LL} = \omega(L_b + L_c)/(r_b + r_c)$. Remembering that D_c is equal to $D_{a,S}$, the SNR of the BWP with LL relative to the SWP can be formulated as

$$\frac{\mathrm{SNR_{LL}}}{\mathrm{SNR_{SWP}}} = \frac{\mathrm{SNR_{LL}}}{\mathrm{SNR_{a,S}}}$$

$$= \sqrt{\frac{r_c}{r_b + r_c}} \cdot \frac{K_{ab}\sqrt{Q_{a,B}Q_b}}{\sqrt{\left(\frac{r_b+r_c}{r_b}\right)(1 + Q_{LL}^2) + K_{ab}^2 Q_{a,B}Q_b}}.$$

$$(23)$$

3 | EXPERIMENTAL VERIFICATION

3.1 | Measurement protocol

We recorded a series of measurements to compare three different Lenz lenses (LL), and an inductively coupled LC resonator with a SWP. For signal transmission, a BWP with 50 mm diameter was exploited as a Tx/Rx coil. The SWP, the coil of the LC resonator, and the inner coil of the LL have the same diameter of 5 mm. The outer diameter of the Lenz lenses is swept from 12.5 mm (small) to 22.5 mm (middle) to 45 mm (big). All test lenses and coils are manufactured on an FR4 substrate with a 35 μm thick copper layer by an external supplier (CONTAG AG, Germany) and are depicted in Figure 7. For all measurements, water was used as a sample. A PMMA sample container with a diameter of 4.5 mm diameter and a height of 2.5 mm resulting in a sample volume of 40 μL is used. The sample is placed in the isocenter of a horizontal bore Bruker BioSpin 94/20 small animal MR scanner at a static field strength of 9.4 T. Before spectra acquisition, an automated shim procedure was applied, which consists of a B_0 map acquisition, a map shim, and an iterative shim. The flip angle was calibrated manually with a nutation spectrum acquisition experiment. The excitation pulse length was swept at an excitation pulse power of 1 W. From the nutation spectra, the probe efficiencies were computed with the gyromagnetic ratio of protons of $\gamma_{1_H} = 42.576$ MHz/T. All water spectra were recorded in one shot (without averaging) at a receiver bandwidth of 10 kHz. All linewidths were approximately constant at 20-30 Hz. The SNRs were determined from the peak height of the water signal and the noise over a 2 ppm region, and the integrals were computed from 8 ppm to 2 ppm for each spectrum via the TopSpin software (Bruker BioSpin GmbH, Germany). The acquired data is summarized in Table 2, which also includes the theoretical (simulation and calculation) results. In addition to that, the table shows the efficiency of each coil configuration computed from the measured flip angle, excitation power, and the length of the excitation pulse.

3.2 | Experimental results

With a high filling factor and minimum transmission losses, the SWP resonator is the most efficient at a measured SNR of 10959. The SNR of the SWP is used as a reference (100% rel. SNR), and subsequently, the SNR values of the other coils and lenses were normalized with respect to it. As expected from the theoretical predictions, the inductively coupled LC resonator exhibited the closest performance to the SWP resonator with a measured relative peak SNR of 78.2%, which perfectly matches the theoretically predicted relative SNR values of 77.3% (simulated) and 78% (calculated). The Tx/Rx BWP measured a relative peak SNR of 12.8% (predicted at 7.2% with simulation and 7.6% with calculation), while the big Lenz lens with an outer diameter of 45 mm showed a relative peak SNR of 25.9% which again matches the values estimated theoretically. Thus, the big Lenz lens approximately doubles the SNR of the Tx/Rx BWP.

On the other hand, the smallest LL with a relative SNR of 0.6% did not present a remarkable enhancement of the BWP's SNR, which is quite unlike the theoretical
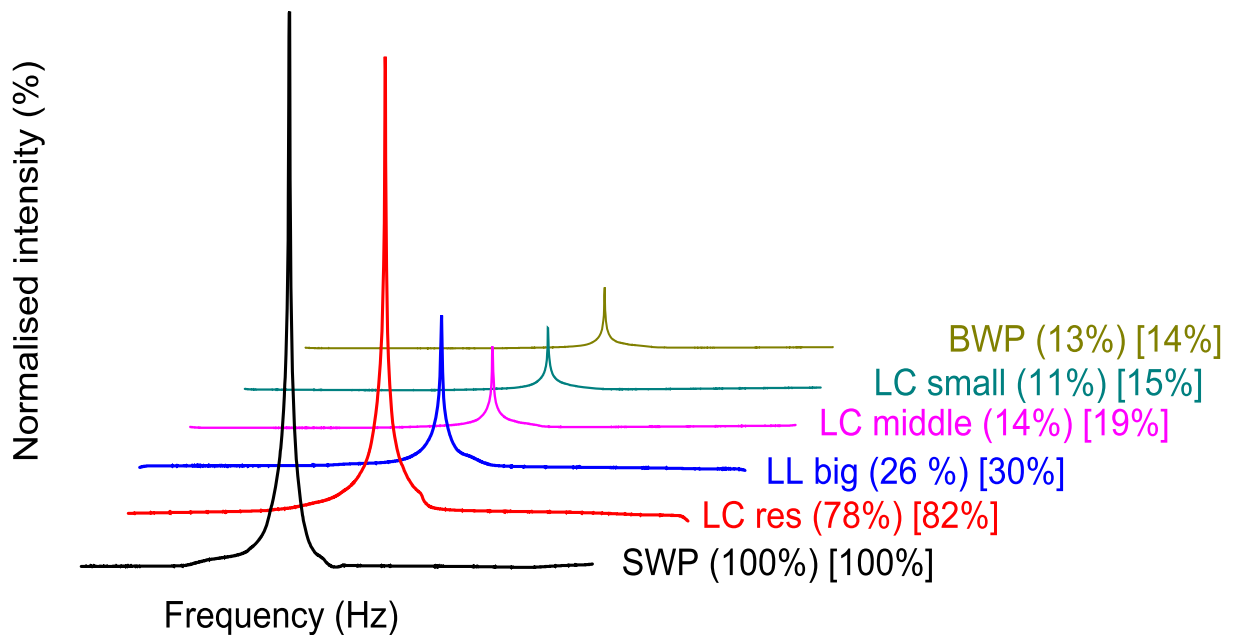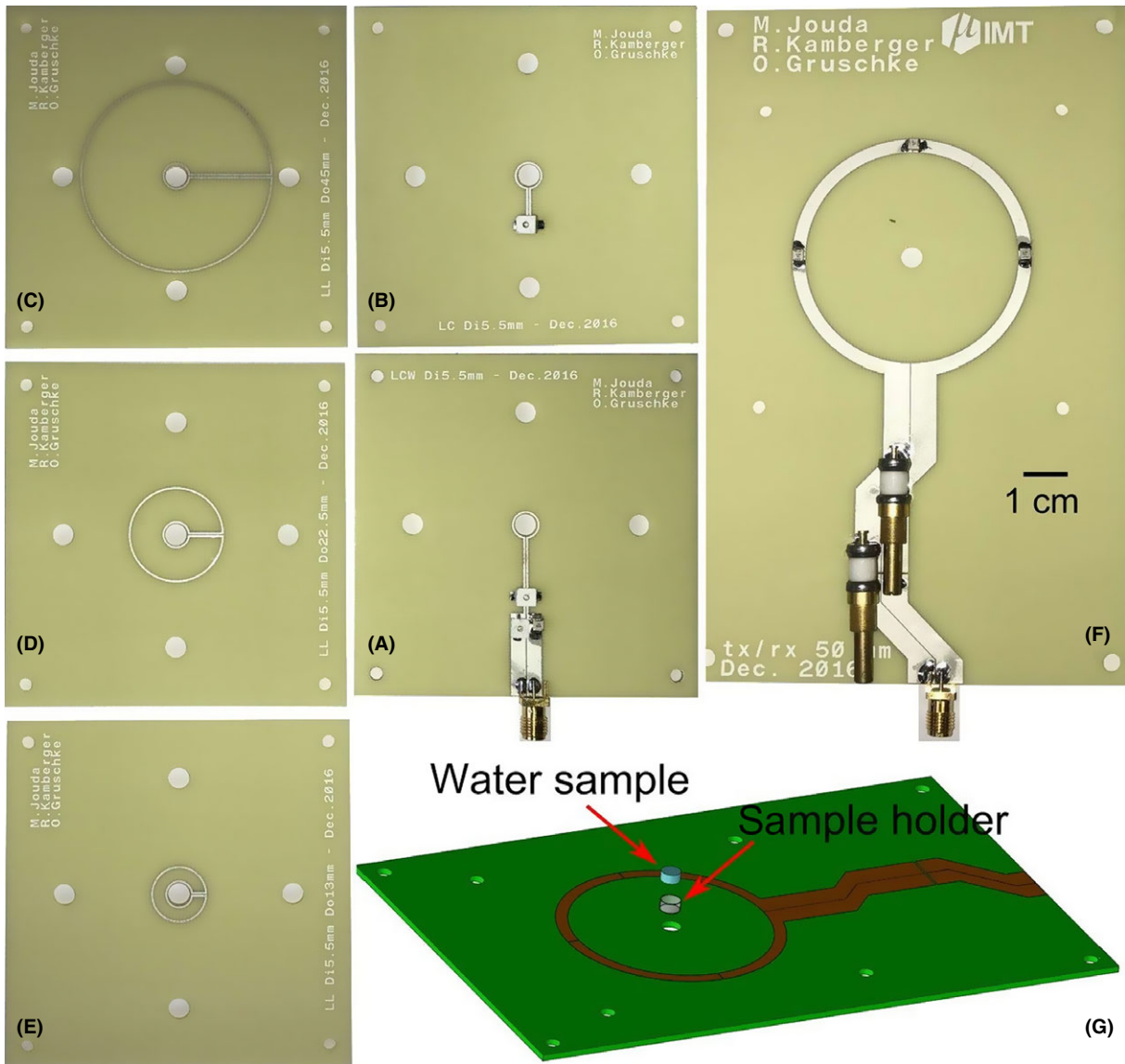
FIGURE 7 Top: Images of (A) the SWP, (B) the LC resonator, (C) the big, (D) the middle, (E) the small lenz lenses with inner coil diameter of 5 mm, (F) the BWP, and (G) the sample holder. Bottom: Collected spectra from a 4.5 mm diameter 40 μL water sample with their normalized intensities in %. The normalized peak SNR values are given in round brackets, while the values for the normalized integrals (integrated from 8 ppm to 2 ppm) are given in square brackets

TABLE 2 Measurement results for different inductively coupled coils with a fixed inner coil diameter (ID) of 5 mm and various outer diameters (OD). The integrals are acquired over from 8 ppm to 2 ppm

	(A) SWP	(B) LC resonator	Lenz Lenses (LL)			(F) BWP
			(C) Big	(D) Middle	(E) Small	
OD/ID in mm/mm	-/5	-/5	45/5	22.5/5	12.5/5	50/-
Mes. Abs. SNR	10 959	8565	2743	1514	1167	1401
Sim. Abs. SNR	11 018	8517	2920	1817	903	793
Mes. Rel. SNR in %	100	78.2	25.9	13.8	10.6	12.8
Sim. Rel. SNR in %	100	77.3	26.5	16.5	8.2	7.2
Cal. Rel. SNR in %	100	78	26.8	14.9	7.5	7.6
Linewidth in Hz	28.7	29.7	36.2	22	19.5	16.8
Efficiency in $\mu T/\sqrt{W}$	167.8	148.8	58.7	24.7	18.8	16.2
Normalized Integrals in %	100	82	30	19	15	14

calculations. We presume this lower performance is owed to the small linewidth of the Tx/Rx BWP. It should be noted that the SNR of the spectra varies with the linewidth, which could not be exactly matched for all measurements, due to the close proximity of the copper conductors for some of the coils and lenses. The integrals are less affected by the linewidth, thus the integral of the small Lenz lens (15%) is marginally better than the Tx/Rx BWP's integral (14%).

4 | CONCLUSION

We simulated and experimentally tested a number of MR coil configurations and reported an extensive comparison of their performance. Namely, these configurations comprised a SWP, a BWP, and a BWP with inductively coupled LC resonator and Lenz lens. As expected, the SWP performs superior to all other coils for the chosen sample, since it has an optimal filling factor as well as the most efficient signal transmission (best B_u/I). Therefore, whenever possible, this coil should be used.

On the other hand when it is not possible to use a coil with optimum coil/sample geometry, then as the coil's size increases with respect to the sample's dimensions the filling factor decreases and, as a result, the sensitivity of the MR probe decreases dramatically. Two candidate solutions can, in such a case, be used to enhance the performance of the BWP. These are the LC resonator and the Lenz lens. The results demonstrated that the LC resonator can achieve a performance close to that of the SWP, which makes it, in

general, preferable to the Lenz lens. However, the simulations and calculations showed that this is true only when the Q of the LC resonator is sufficiently high, and the resonance hits exactly the Larmor frequency. These requirements of high Q and exact resonance at the Larmor frequency are hard to satisfy simultaneously, since the higher the Q the larger the resonance split and thus the more tricky is the tuning and matching. Nevertheless, a reasonable compromise can usually be found.

In contrast, the Lenz lens shows inherently lower performance than the LC resonators. In best cases, it can improve the SNR of the BWP up to 30% of the optimum achievable SNR of the SWP. This renders it less attractive in general. Nevertheless, considering its broadband nature and its ability to focus, shape, and even reorient the B_u field, the LL can be beneficial in multinuclear experiments and implantable devices in which cases direct wire connections and bulky tuning capacitors are not feasible.

ORCID

Mazin Jouda http://orcid.org/0000-0002-1226-1174
Robert Kamberger http://orcid.org/0000-0001-5915-5769
Jürgen Hennig http://orcid.org/0000-0002-2273-3497
Jan G. Korvink http://orcid.org/0000-0003-4354-7295

REFERENCES

1. Traficante DD. Impedance: what it is, and why it must be matched. *Concepts Magn Reson*. 1989;1:73-92.
2. Hoult D, Tomanek B. Use of mutually inductive coupling in probe design. *Concepts Magn Reson*. 2002;15:262-285.
3. Decorps M, Blondet P, Reutenauer H, Albrand J, Remy C. An inductively coupled, series-tuned NMR probe. *J Magn Reson (1969)*. 1985;65:100-109.
4. Froncisz W, Jesmanowicz A, Kneeland JB, Hyde JS. Counter rotating current local coils for high-resolution magnetic resonance imaging. *Magn Reson Med*. 1986;3:590-603.
5. Kuhns PL, Lizak MJ, Lee S-H, Conradi MS. Inductive coupling and tuning in NMR probes; applications. *J Magn Reson (1969)*. 1988;78:69-76.
6. Utsuzawa S, Mandal S, Song Y-Q. Transformer-coupled NMR probe. *J Magn Reson*. 2012;216:128-133.
7. Bilgen M, Elshafiey I, Narayana PA. In vivo magnetic resonance microscopy of rat spinal cord at 7 T using implantable RF coils. *Magn Reson Med*. 2001;46:1250-1253.
8. Couty M, Nazeer S, Jelita C, et al. Ultra-flexible micro-antennas on PDMS substrate for MRI applications, in Design, Test, Integration and Packaging of MEMS/MOEMS (DTIP), 2012 Symposium on, pp. 126-131, IEEE, 2012.
9. Ginefri J-C, Rubin A, Tatoulian M, et al. Implanted, inductively-coupled, radiofrequency coils fabricated on flexible polymeric material: application to in vivo rat brain MRI at 7 T. *J Magn Reson*. 2012;224:61-70.
10. Wirth E III, Mareci T, Beck B, Fitzsimmons J, Reier P. A comparison of an inductively coupled implanted coil with optimized surface coils for in vivo NMR imaging of the spinal cord. *Magn Reson Med*. 1993;30:626-633.
11. Quick HH, Kuehl H, Kaiser G, Bosk S, Debatin JF, Ladd ME. Inductively coupled stent antennas in MRI. *Magn Reson Med*. 2002;48:781-790.
12. Schnall M, Barlow C, Subramanian VH, Leigh J. Wireless implanted magnetic resonance probes for in vivo NMR. *J Magn Reson (1969)*. 1986;68:161-167.
13. Silver X, Ni WX, Mercer E, et al. In vivo 1H magnetic resonance imaging and spectroscopy of the rat spinal cord using an inductively-coupled chronically implanted RF coil. *Magn Reson Med*. 2001;46:1216-1222.
14. Marsden B, Lim V, Taber B, Zens A. Improving the mass-limited performance of routine NMR probes using coupled coils. *J Magn Reson*. 2016;268:25-35.
15. Jacquinot J-F, Sakellariou D. NMR signal detection using inductive coupling: applications to rotating microcoils. *Concepts Magn Reson*. 2011;38:33-51.
16. Sakellariou D, Le Goff G, Jacquinot J-F. High-resolution, high-sensitivity NMR of nanolitre anisotropic samples by coil spinning. *Nature*. 2007;447:694-697.
17. Ryan H, Song S-H, Zaß A, Korvink J, Utz M. Contactless NMR spectroscopy on a chip. *Anal Chem*. 2012;84:3696-3702.
18. Tang JA, Jerschow A. Practical aspects of liquid-state NMR with inductively coupled solenoid coils. *Magn Reson Chem*. 2010;48:763-770.
19. Utz M, Monazami R. Nuclear magnetic resonance in microfluidic environments using inductively coupled radiofrequency resonators. *J Magn Reson*. 2009;198:132-136.
20. Vassiliou C, Liu V, Cima M. Miniaturized, biopsy-implantable chemical sensor with wireless, magnetic resonance readout. *Lab Chip*. 2015;15:3465-3472.
21. Volland NA, Mareci TH, Constantinidis I, Simpson NE. Development of an inductively coupled MR coil system for imaging and spectroscopic analysis of an implantable bioartificial construct at 11.1 T. *Magn Reson Med*. 2010;63:998-1006.
22. Wang T, Ciobanu L, Zhang X, Webb A. Inductively coupled RF coil design for simultaneous microimaging of multiple samples. *Concepts Magn Reson*. 2008;33:236-243.
23. Terman FE. *Radio engineers' handbook*. New York, NY: McGraw-Hill; 1943.
24. Hartmann S, Hahn E. Nuclear double resonance in the rotating frame. *Phys Rev*. 1962;128:2042.
25. Cross V, Hester R, Waugh J. Single coil probe with transmission-line tuning for nuclear magnetic double resonance. *Rev Sci Instrum*. 1976;47:1486-1488.
26. Bornet A, Melzi R, Perez Linde AJ, et al. Boosting dissolution dynamic nuclear polarization by cross polarization. *J Phys Chem Lett*. 2012;4:111-114.
27. Schoenmaker J, Pirota K, Teixeira J. Magnetic flux amplification by lenz lenses. *Rev Sci Instrum*. 2013;84:085120.
28. Hoult DI, Richards R. The signal-to-noise ratio of the nuclear magnetic resonance experiment. *J Magn Reson (1969)*. 1976;24:71-85.